THE JOURNAL OF PHYSICAL CHEMISTRY C

Article

pubs.acs.org/JPCC

Structure and Surface Reactivity of WO_4^{2-}, SO_4^{2-}, PO_4^{3-} Modified Ca-Hydroxyapatite Catalysts and Their Activity in Ethanol Conversion

Kanaparthi Ramesh,*[,†,⊥] Eileen Goh Yi Ling,[‡] C. G. Gwie,[†] Timothy J. White,[‡,§] and Armando Borgna[†]

[†]Institute of Chemical and Engineering Sciences (ICES), 1, Pesek Road, Jurong Island, 627833, Singapore

[‡]School of Materials Science and Engineering, Nanyang Technological University, Block N4.1, 50 Nanyang Avenue, 639798, Singapore

[§]Australian National University, Electron Centre for Advanced Microscopy, GPO Box 475, Canberra, ACT 2601, Australia

[⊥]HPCL Corporate R&D Centre, First Floor, Adarsh Eco Place, 176 EPIP, Kundenahalli Hobli, Whitefield, Bangalore, 560 066 India

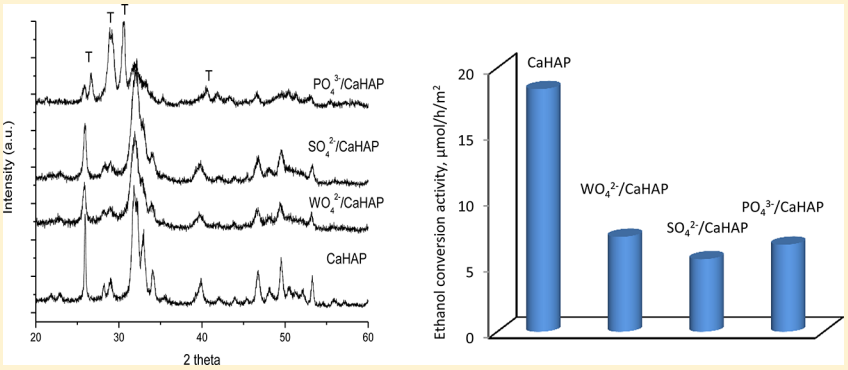

ABSTRACT: In the current study, we have synthesized calcium hydroxyapatite (CaHAP) from different phosphorus sources namely, $NH_4H_2PO_4$ and H_3PO_4. The structure of CaHAP was confirmed by XRD, FT-IR, and Raman characterization methods. The CaHAP was further modified with various anions such as WO_4^{2-}, SO_4^{2-}, and PO_4^{3-} with fixed content of 10 wt %. To understand the textural and structural properties, these samples were thoroughly characterized by N_2 physisorption, X-ray diffraction, Fourier transform infrared, Raman and thermogravimetry−differential thermal analysis methods. Ethanol adsorption at various temperatures was studied in detail using diffuse reflectance Fourier transform spectroscopic to unravel the formation and stability of surface species and the interaction of ethanol with CaHAP. The temperature programmed desorption of ethanol (ethanol-TPD) was performed to understand the stability, surface reactivity, and product distribution. The catalytic activity of the above catalysts was tested in ethanol conversion over a temperature range of 300−450 °C.

1.0. INTRODUCTION

Calcium hydroxyapatite (CaHAP; $Ca_{10}(PO_4)_6(OH)_2$) is currently attracting considerable interest for applications in chromatography,[1] bioengineering,[2] and catalysis.[3−7] The utility of this material can be broadened by partial replacement of Ca^{2+} ions with transvalent metal ions (usually, M^{2+} and M^{3+}) and substitution of PO_4^{3-} ions with suitable anions.[7] Consequently, CaHAP can be tailored as an active solid catalyst or support with readily tunable surface properties. Metal (Ru, Ni, Co) modified CaHAP catalysts were found to be active catalysts in the water gas shift reaction,[8] partial oxidation of methane to syngas,[9] and oxidative dehydrogenation of ethane.[10] Recently, metals incorporated hydroxyapatites have been widely reported for various catalytic applications; however, less attention has been paid to the incorporation of anions in the CaHAP framework and further study of the surface reactivity of these solids.

CaHAP crystallizes with hexagonal *P*63/*m* symmetry with Ca^{2+} ions arranged in two nonequivalent sites, that is, Ca(I) and Ca(II) ions. Ca(I) ions are aligned in columns, whereas Ca(II) ions are in equilateral triangles centered on an axis surrounded with PO_4^{3-} tetrahedra. CaHAP exhibits both acid and base properties in its crystal lattice accompanied by important properties such as high adsorption capacity and ion-exchange capabilities. Because of their beneficial surface properties, CaHAP catalysts have been applied in the dehydrogenation and dehydration of alcohols.[11,12] Conversion of bio-alcohols, especially bio-ethanol, into value-added chemicals is an industrially important reaction, currently attracting interest. Tsuchida et al.[13] reported the ethanol conversion over a nonstoichiometric CaHAP catalyst to form higher alcohols by the Guebert reaction. The synthesis of biogasoline from ethanol with high selectivity in a one step-process on highly active nonstoichiometric hydroxyapatite was also reported.[14]

Received: May 1, 2012
Revised: July 11, 2012
Published: August 1, 2012

   dx.doi.org/10.1021/jp304187v | *J. Phys. Chem. C* 2012, 116, 18736−18745

The PO_4^{3-} groups in the apatite framework can be replaced by vanadates (VO_4^{3-}), arsentates (AsO_4^{3-}), and chromates (CrO_4^{2-}).[15−17] Ogo et al.[18] have applied the vanadate substituted hydroxyapatite for the catalytic conversion of 2-propanol. The catalytic activities of vanadate hydroxyapatites were found to be higher than those of phosphate hydroxyapatites. Onda et al.[19] reported the synthesis of vanadate-substituted hydroxyapatites by a simple hydrothermal synthesis at relatively low temperature using alkaline media. It has been reported that the surface P−OH groups can be modified with pyrophosphoric acid ($H_4P_2O_7$) treatment on CaHAP surfaces resulting in additional P−OH groups.[20] From these reports, it is clear that the anions are able to modify the CaHAP surface by entering into the apatite framework, thereby influencing the surface reactivity.

Stoichiometric CaHAP (molar ratio of Ca/P 1.67) possesses mainly basic sites, while the nonstoichiometric CaHAP (molar ratio of Ca/P 1.50 to 1.65) exhibits predominantly acid properties.[21] Thus, nonstoichiometric CaHAP can act as a solid acid suitable for the dehydration of ethanol to ethylene, while stoichiometric CaHAP catalyzes ethanol dehydrogenation to produce acetaldehyde. Surface P−OH groups play an important role in tuning properties such as dispersion of nanoparticles on CaHAP.[22] Methanol adsorption and dehydrogenation over stoichiometric and nonstoichiometric hydroxyapatite catalysts has been reported in the literature.[21] On stoichiometric CaHAP (Ca/P = 1.65) methanol decomposes only at 600 °C to produce CO. However, the selectivities toward formaldehyde and dimethyl ether were increased at low Ca/P ratio (1.51). To our knowledge, the comparative study to investigate the influence of anions such as WO_4^{2-}, SO_4^{2-}, and PO_4^{3-} on CaHAP to understand the surface structure and reactivity has not been undertaken. In this contribution, we studied the ethanol adsorption and conversion on CaHAP and the influence of anion (WO_4^{2-}, SO_4^{2-}, and PO_4^{3-}) modification during ethanol conversion.

Hence, in the present work, we report on the impact of anion modification using WO_4^{2-}, SO_4^{2-}, and PO_4^{3-} on the CaHAP structure together with the surface reactivity of the modified catalysts. In addition, the adsorption of ethanol on CaHAP and anion modified CaHAP at various temperatures and treatment conditions using DRIFT was systematically investigated. In the current study, in situ diffuse reflectance infrared fourier transform spectroscopy (DRIFTS) and temperature programmed desorption of ethanol (Ethanol- TPD) were employed to understand the adsorption and surface reactivity of ethanol. The catalysts were thoroughly characterized using X-ray diffraction (XRD), Fourier transform infrared spectroscopy (FT-IR) and thermal gravimetric analysis (TGA).

2.0. EXPERIMENTAL SECTION

2.1. Preparation of the Calcium Hydroxyapatite Samples. Stoichiometric CaHAP ($Ca_{10}(PO_4)_6(OH)_2$) with Ca/P of 1.67 was synthesized in pure phase from $NH_4H_2PO_4$ and H_3PO_4 precursors by a coprecipitation method. The CaHAP synthesized from $NH_4H_2PO_4$ was further used for modification with anions such as WO_4^{2-}, SO_4^{2-}, and PO_4^{3-}. Details of the individual preparation methods are described below.

CaHAP Using $NH_4H_2PO_4$ as Precursor. A solution of calcium nitrate tetrahydrate ($Ca(NO_3)_2{\cdot}4H_2O$) (6.67×10^{-2} mol) in 60 mL of H_2O was prepared and brought to pH 11−12 with aqueous NH_3 (4.98 N) addition and further diluted to 120 mL. A solution of ammonium dihydrogen phosphate ($NH_4H_2PO_4$) (4.00×10^{-2} mol) in 100 mL of H_2O was prepared and brought to pH 11−12 with aqueous NH_3 (4.98 N) and thereafter diluted to 160 mL. The calcium solution was vigorously stirred at room temperature, and the phosphate solution was added dropwise over *ca.* 30 min to produce a milky, gelatinous precipitate which was stirred and boiled at 70 °C for 1 h. The precipitate was filtered, washed, dried at 80 °C overnight, and then calcined at 500 °C for 3 h. The preparation reaction can be explained as follows:

$$6(NH_4)H_2PO_4 + 10Ca(NO_3)_2 + 14NH_4OH \rightarrow Ca_{10}(PO_4)_6(OH)_2 + 20NH_4NO_3 + 12H_2O$$

CaHAP with H_3PO_4 as Precursor. A solution of $Ca(NO_3)_2{\cdot}4H_2O$ (6.67×10^{-2} mol) in 60 mL H_2O was prepared and brought to pH 11−12 with aqueous NH_3 (4.98 N) and further diluted to 120 mL. A solution of phosphoric acid (H_3PO_4, 85%) (4.00×10^{-2} mol) with corresponding weight of 4.612 g in 100 mL of H_2O was prepared and brought to pH 11−12 with aqueous NH_3 (4.98 N) and further diluted to 160 mL. The calcium solution was vigorously stirred at room temperature, and the phosphoric acid was introduced dropwise over ca. 30 min to yield a gelatinous precipitate that was stirred with boiling (70 °C for 1 h). This product was filtered, washed, dried (80 °C overnight), and calcined at 500 °C for 3 h to crystallize CaHAP. This preparation can be expressed as follows:

$$6H_3PO_4 + 10Ca(NO_3)_2 + 10NH_4OH \rightarrow Ca_{10}(PO_4)_6(OH)_2 + 10NH_3(NO_3)_2 + 8H_2O + H_2$$

SO_4^{2-}/CaHAP (10 wt % SO_4^{2-}). Calcined CaHAP was impregnated with 0.5 M of H_2SO_4 and diluted with 15 mL of deionized water. This suspension was mechanically stirred for 2 h. Then, the precipitate was filtered, washed, dried at 120 °C overnight and calcined at 500 °C for 4 h with a heating rate of 10 °C/min.

WO_2^{4-}/CaHAP (10 wt % WO_3). To prepare 1 g of 10 wt % of WO_3 on CaHAP, a solution of sodium tungstate dihydrate ($Na_2WO_4{\cdot}2(H_2O)$) containing 0.156 g of this salt was prepared with 5 mL of H_2O. CaHAP was impregnated with this solution. The slurry was well mixed on a roller, and thereafter left drying 120 °C overnight and calcined at 500 °C for 4 h with a heating rate of 10 °C/min.

PO_4^{3-}/CaHAP (10 wt % PO_4). To synthesize 1 g of 10 wt % PO_4 on CaHAP, a calculated amount of H_3PO_4 (85%) was diluted with 0.667 mL of H_2O. Calcined CaHAP was treated with the H_3PO_4 solution. The sample was left to mix well on the roller, and thereafter was left to dry at 120 °C overnight, followed by calcination at 500 °C for 4 h with a heating rate of 10 °C/min.

2.2. Catalyst Characterization. The powder XRD profiles were collected from 2 to 60° 2θ using CuKα with a Bruker D8 X-ray diffractometer. Thermal gravimetric analysis experiments were conducted using a Setaram Setsys Evolution 12 thermobalance with a nitrogen dynamic flow of 140 mL (NTP)/min. The sample weight and temperature were monitored as a function of time. About 10−30 mg of catalyst was used for each experiment.

FT-IR spectra were recorded on a Bio-Rad FT-IR 3000 MX, FT-IR spectrometer, in the range of 4000 to 400 cm^{-1}. In a typical analysis, approximately 25 mg of the sample and 1 g of

dx.doi.org/10.1021/jp304187v | J. Phys. Chem. C 2012, 116, 18736−18745

KBr was weighed, milled, and ground in an agate mortar, until a fine smooth powder of even particle size was obtained. About 250 mg of the sample and KBr mixture was pressed with a steel die into a pellet.

In situ DRIFTS analysis was carried out on a BIO-RAD spectrometer (Excalibur series, FTS 3000) equipped with a MCT detector and a high temperature DRIFT cell fitted with KBr windows. The spectra were acquired with a resolution of 4 cm^{-1}. Typically 256 scans were recorded, averaged, and transformed by the Kubelka–Munk algorithm using KBr as a reference material. Typically, about 20 mg of sample was loaded into the DRIFTS cell without further dilution. Subsequently, spectra were recorded in helium flow in the temperature range between ambient to 400 °C. The sample was heated at 400 °C for 2 h in a dynamic He flow (UHP, 99.999%) of 20 mL/min. Ethanol was adsorbed on the treated catalysts for about 15 min and the spectra were collected at various adsorption temperatures.

Raman spectra were collected with a dispersive Raman microscope (Bruker Senterra) equipped with a thermoelectrically (TE) cooled CCD array detector and a high-grade Leica microscope using a 50× objective. The spectra were measured using a neon ion laser (532 nm) with a laser power of 20 mW, where each spectrum was an average of 3 scans with a measurement time of 10 s per scan. The Raman spectral measurements were performed confocally and the spectra were subsequently baseline corrected.

To understand the surface reactivity, ethanol-TPD was conducted from ambient temperature to 500 °C. Prior to ethanol adsorption, the sample was treated at 400 °C for 2 h in the continuous flow of helium (50 mL/min). Subsequently, ethanol was adsorbed on the CaHAP catalysts for 1 h at room temperature and the desorption of ethanol and formation of various products (acetaldehyde, ethylene, diethyl ether, acetone, CO_2, CO, and H_2) in contact with the CaHAP surface were monitored using an online portable mass spectrometer (HIDEN Analytical) using Quantal software for the normalization. Similar experiments were also conducted on WO_4^{2-}, SO_4^{2-}, and PO_4^{3-} modified CaHAP samples.

The ethanol dehydration reaction was carried out in a vertical fixed bed continuous down-flow steel microreactor under atmospheric pressure. In a typical experiment, about 500 mg of the catalyst was diluted with equal volume of quartz grains and packed between two layers of quartz wool in the reactor. The upper portion of the reactor was filled with quartz beads that served both as a preheater and a mixer for the reactants. Prior to introducing the reactant, the catalyst was treated in nitrogen flow at a rate of 20 mL/min for 4 h at 500 °C. The reaction temperature was monitored by a thermocouple with its tip located in the catalyst bed and connected by a PID-type temperature indicator-controller. Catalytic tests were performed by injecting ethanol (HPLC grade) and its diluted solutions with HPLC infusion pump (Agilent 1100 series). The reaction was carried out at various temperatures ranging from 300 to 450 °C. Prior to introduction into the reactor, ethanol was mixed with helium at 175 °C. The gaseous products, after the catalyst had attained a steady state, were analyzed by an online gas chromatograph (Agilent 6890) equipped with flame ionization detector (FID) using a HP-5 capillary column. Liquid products were condensed at 0 °C and analyzed using a GC–MS (Agilent 6890).

3.0. RESULTS AND DISCUSSION

Structural and Textural Properties. XRD patterns of CaHAP synthesized from $NH_4H_2PO_4$ and H_3PO_4 calcined at 500 °C are shown in Figure 1a. CaHAP synthesized from both precursors yielded well-crystalline CaHAP with characteristic reflections at 2θ = 49.48, 46.78, 39.76, 32.94, 31.85, and 25.93° corresponding d values at 1.84, 1.94, 2.26, 2.71, 2.80, and 3.43 Å being consistent with a space group $P63/m$. It can also be observed that a very sharp reflection at 2θ = 25.93° (002) compared to the others indicates the formation of CaHAP with acicular needle shape.

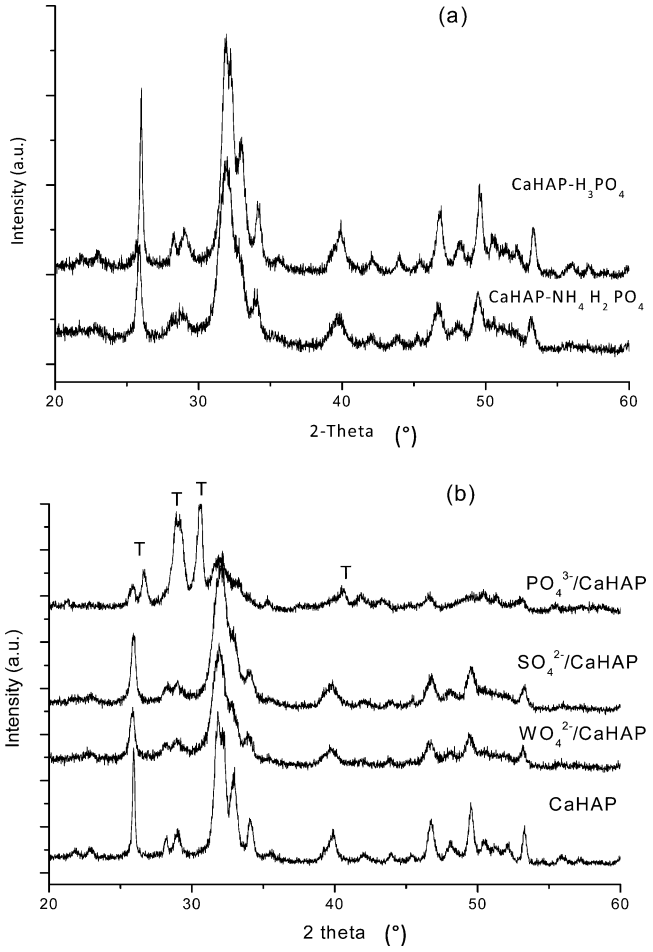

Figure 1. XRD profiles of (a) hydroxyapatites synthesized from $NH_4H_2PO_4$ and H_3PO_4 precursors, (b) hydroxyapatites modified with WO_4^{2-}, SO_4^{2-}, PO_4^{3-} (T = tricalcium phosphate ($Ca_3(PO_4)_2$).

XRD profiles of WO_4^{2-}, SO_4^{2-}, and PO_4^{3-} modified CaHAP samples are shown in Figure 1b. The XRD profiles of pure CaHAP and SO_4^{2-}, and WO_4^{2-} modified CaHAP samples exhibited similar features, and no crystalline features due to WO_3 were observed. The absence of a peak at 2θ = 24.2° (d = 3.67 Å) indicates that the WO_3 is either well dispersed or completely substituted in the CaHAP lattice. For the PO_4^{3-} modified CaHAP sample, in addition to the CaHAP reflections, additional intense peaks at 2θ = 30.6 and 26.5°, corresponding to d values at 2.92 and 3.36 Å, were also observed. These additional features can be attributed to β-tricalcium phosphate, (β-$Ca_3(PO_4)_2$). It should be noted that PO_4^{3-}/CaHAP profile shows less intense diffraction peaks for the CaHAP phase including the characteristic peak at 2θ = 31.85 (211), indicating

dx.doi.org/10.1021/jp304187v | J. Phys. Chem. C 2012, 116, 18736–18745

the low crystallinity of the CaHAP phase. It should be also noted here that the characteristic reflections due to the apatite structure still exist along with the major β-$Ca_3(PO_4)_2$ structure. The transformation of CaHAP to β-$Ca_3(PO_4)_2$ (TCP) occurs at high temperature (>1100 °C) and can be expressed by eq 1.[23] In the current study, we could explain the formation of $Ca_3(PO_4)_2$ by the surface reaction between CaHAP and H_3PO_4 at significantly lower temperatures (500 °C) as shown in eq 2.

$$Ca_{10}(PO_4)_6(OH)_2 \rightarrow 3Ca_3(PO_4)_2 + CaO + H_2O \quad (1)$$

$$2Ca_{10}(PO_4)_6(OH)_2 + 2H_3PO_4 \rightarrow 6Ca_3(PO_4)_2 + Ca_2P_2O_7 + 5H_2O \quad (2)$$

It can also be observed that PO_4^{3-} modified CaHAP shows strong reflections due to β-TCP suggesting the potential dissolution of CaHAP and recrystallization as β-TCP with a loss of partial Ca in the solid solution.

N_2 physisorption results obtained at −196 °C for pure CaHAP and anion-modified CaHAP are presented in Table 1.

Table 1. N_2 Physisorption Results of CaHAP and WO_4^{2-}, SO_4^{2-}, PO_4^{3-} Modified CaHAP Catalysts

sample	surface area (m^2/g)	pore volume, $\times10^{-2}$, (mL/g)	external surface area (m^2/g)[a]	micropore volume $\times10^{-2}$ (mL/g)[a]
CaHAP	72	3.01	64	0.42
WO_4^{2-}/CaHAP	59	2.43	53	0.28
SO_4^{2-}/CaHAP	106	4.34	99	0.31
PO_4^{3-}/CaHAP	53	2.17	50	0.13

[a]External surface area and micropore volume were determined by t-method.

The specific surface area of pure CaHAP is found to be 72 m^2/g and decreased with the addition of PO_4^{3-} and WO_4^{2-} anions to 53 and 59 m^2/g, respectively. This clearly suggests that PO_4^{3-} species are strongly reacting with the surface thereby decreasing the surface area by forming narrow CaHAP pore channels, whereas the decrease in the surface area of CaHAP by the addition of WO_4^{2-} species can be attributed to high atomic weight of W. Interestingly, the surface area was found to increase for SO_4^{2-} modified CaHAP sample from 72 to 106 m^2/g. The total pore volume (mL/g) measured by Barret−Joyner−Halenda (BJH) method also followed a similar trend. Other textural details obtained by N_2 physisorption such as external surface area and micropore volume measured by the t-method are also presented in Table 1.

Thermal Stability of Anion Modified CaHAp. The thermal gravimetric analysis of various CaHAP samples synthesized from H_3PO_4 and $NH_4H_2PO_4$ precursors shows quite different weight loss patterns (Figure 2a,b). CaHAP prepared from $NH_4H_2PO_4$ showed gradual weight loss at low temperatures (≤150 °C) and displayed a sharp weight loss between 150 and 250 °C. Above this temperature, a gradual weight loss between 250 and 750 °C was observed. The weight loss at 218 °C can be attributed to the decomposition of $NH_4H_2PO_4$ to H_3PO_4 with evolution of NH_3 gas. In contrast, the CaHAP prepared from H_3PO_4 precursor has a sharp weight loss between ambient and 60 °C and a very gradual decline above 60 °C until 390 °C; above this temperature little change in weight was observed. Derivative weight loss patterns show maxima at 218 and 700 °C for CaHAP prepared from $NH_4H_2PO_4$. In contrast, derivative weight loss maxima at 32 and 705 °C were observed for CaHAP prepared from H_3PO_4. The high temperature endothermic peak at around 700 °C is attributed to the decarbonation of $CaCO_3$.[24] The slow elimination of carbonate groups at this temperature is linked to the CaHAP lattice.[25] The low temperature weight loss can be attributed to the gradual loss of adsorbed water (below 200 °C) and loss of irreversible lattice water between 200 −400 °C. Interestingly, the total weight loss (%) was found to be similar (nearly 15%) for both CaHAP samples. These results clearly show the high thermal stability of CaHAP samples above 400 °C up to 700 °C.[26]

The thermal gravimetric analysis profiles of WO_4^{2-}, SO_4^{2-}, and PO_4^{3-} modified CaHAP samples are shown in Figure 2 panels c, d, and e, respectively. The WO_4^{2-} and PO_4^{3-} modified CaHAP samples showed 13% weight loss compared to only 5.5% observed for SO_4^{2-}/CaHAP sample. The WO_4^{2-}/CaHAP sample shows three regions of weight losses between 80 and 225 °C, 235 and 475 °C and 475 and 677 °C, exhibiting derivative weight loss peaks at around 218 (s), 422 (b), and 673 (s) °C. SO_4^{2-}/CaHAP shows two regions of weight losses in the temperature ranges of 80−430 and 430−700 °C, respectively. In the high temperature range, a sharp derivative peak centered at 698 °C (s) is observed. In contrast, the PO_4^{3-}/CaHAP sample shows five weight loss regions in the following temperature ranges: 80−120, 120−225, 225−370, 370−440, and 440−743 °C with corresponding derivative peaks centered at 191(s), 330, 410(s), 714 °C(s). The low temperature weight loss below 225 °C is due to the release of physisorbed and structural water while the high temperature endothermic peaks correspond to the condensation of H_xPO_y species and their structural transformations.[27] The decomposition temperature of H_3PO_4 corresponds to 158 °C and the corresponding peak indicating the structural transformation can be seen between 145 and 255 °C. The high temperature peaks at 191, 330, and 410 °C can be attributed to the surface transformation of CaHAP reacting with H_3PO_4 corresponding to the following equations (eq 4−eq 6) to form $Ca_3(PO_4)_2$.

$$Ca_{10}(PO_4)_6(OH)_2 + 2H_3PO_4 \rightarrow Ca_{10-x}(HPO_4)_x(PO_4)_{6-x}(OH)_2 \quad (4)$$

$$Ca_{10-x}(HPO_4)_x(PO_4)_{6-x}(OH)_2 \rightarrow Ca_{10-x}(P_2O_7)_x(PO_4)_{6-x}(OH)_2 \quad (5)$$

$$P_2O_7^{4-} + 2OH^- \rightarrow 2PO_4^{3-} + H_2O \quad (6)$$

The low temperature peaks below 180 °C can be ascribed to loss of water followed by the dehydration of HPO_4^{2-} into pyrophosphates.[28] The high temperature loss at 714 °C can be attributed the reaction of OH^- ions of apatite and the pyrophosphate ions formed at lower temperature to form PO_4^{3-} with loss of water as shown in eq 6.

Structure of Various CaHAP Samples. Figure 3a shows the transmission FT-IR spectra of pure CaHAP synthesized from H_3PO_4 and $NH_4H_2PO_4$ sources from 400 to 1500 cm^{-1}. The characteristic absorption bands of CaHAP are invariably present, as compared to CaHAP prepared from $NH_4H_2PO_4$, the CaHAP synthesized from H_3PO_4 showed very less intense carbonate signatures at 1400 and 1450 cm^{-1}.[29,30] Carbonate species might be introduced by the adsorption of atmospheric

dx.doi.org/10.1021/jp304187v | J. Phys. Chem. C 2012, 116, 18736−18745

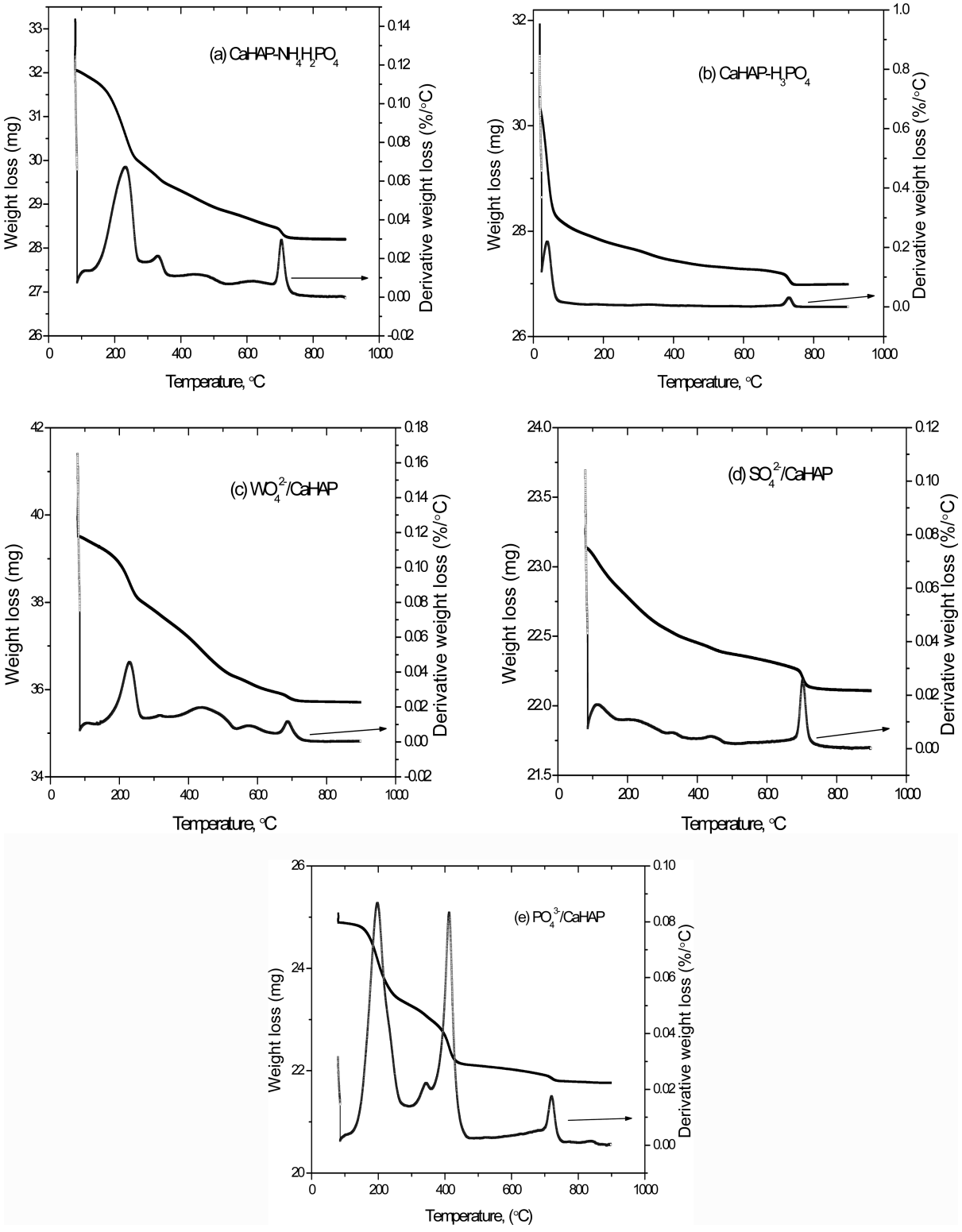

Figure 2. TG analysis of various hydroxyapatites samples: (a) CaHAP synthesized from NH_4 H_2 PO_4; (b) CaHAP synthesized from H_3PO_4; (c) WO_4^{2-}/CaHAP; (d) SO_4^{2-}/CaHAP; and (e) PO_4^{3-}/CaHAP.

CO_2 during the preparation, and may partially displace lattice PO_4^{3-}. Specifically, the synthesized CaHAP exhibited characteristic bands at 470, 560, 604, 630, 958, 1034, 1097, and 1385 cm^{-1}. The band at 1385 cm^{-1}, which can be assigned to nitrate $\upsilon_s(NO_2^-)$ species, is only observed in the case of CaHAP prepared from $NH_4H_2PO_4$. The presence of this band in the CaHAP synthesized using $NH_4H_2PO_4$ as phosphorus source suggests the oxidation of NH_4 group to NO_x during the calcination. The rest of IR bands can be assigned as follows: 630 cm^{-1} to bending mode of OH^- group; P−O stretching modes at 1090 and 1030 ($\upsilon 3$) and 960 cm^{-1} ($\upsilon 1$); O−P−O bending modes at 600 and 565 cm^{-1} ($\upsilon 4$) and 470 cm^{-1} ($\upsilon 2$). The bands at 565 and 600 cm^{-1} are due to PO_4^{3-} bending modes with $\upsilon 4$ symmetry. Additionally, two bands at 1640 and

dx.doi.org/10.1021/jp304187v | J. Phys. Chem. C 2012, 116, 18736−18745

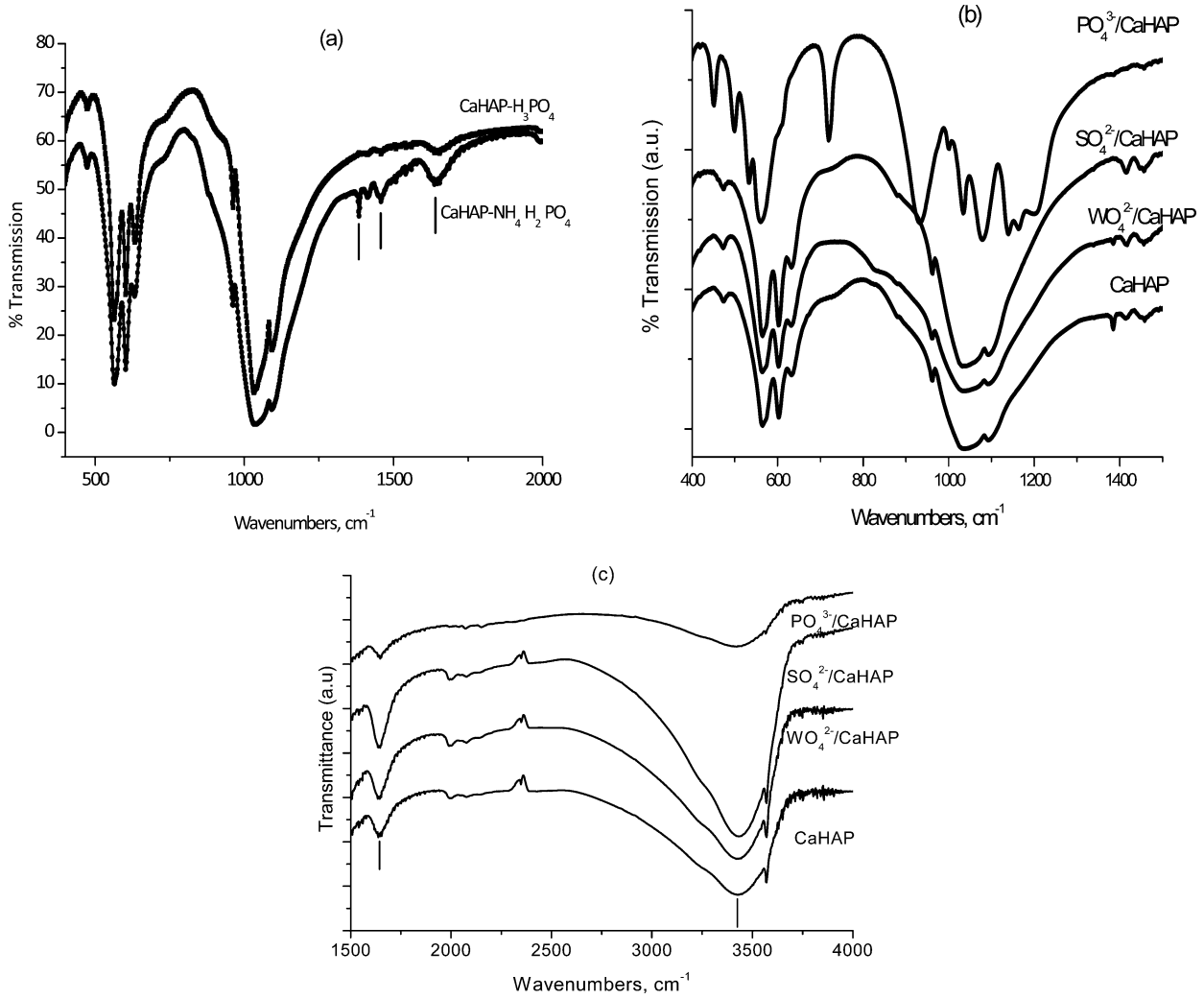

Figure 3. FT-IR analysis of (a) hydroxyapatites synthesized from $NH_4H_2PO_4$ and H_3PO_4 precursors, (b) hydroxyapatites modified with WO_4^{2-}, SO_4^{2-}, PO_4^{3-}, (c) hydroxyapatites modified with WO_4^{2-}, SO_4^{2-}, PO_4^{3-} (1500−4000 cm^{-1}).

3440 cm^{-1} are due to adsorbed water. The band at 875 cm^{-1}, due to HPO_4^{2-} is absent in the spectra obtained for both precursors. HPO_4^{2-} ions can yield pyrophosphates ($P_2O_7^{4-}$) by condensation.[31]

FT-IR spectra of WO_4^{2-}, SO_4^{2-}, and PO_4^{3-} modified CaHAP samples are shown in Figure 3b. In contrast, the IR spectra of PO_4^{3-}/CaHAP showed additional peaks at 448, 498, 530, 720, 927, 1000, 1078, 1140, 1160, and 1205 cm^{-1}, clearly indicating a surface modification by PO_4^{3-} treatment. The presence of several kinds of phosphate groups in the sample can be identified. Owing to the broad nature of the peak at 927 cm^{-1}, it is difficult to rule out any peak around 875 cm^{-1}, which could be attributed to HPO_4^{2-} ions. The peaks around 720, 927, and 1200 cm^{-1} can be ascribed to pyrophosphates.[32] This result agrees well with the TG analysis data that indicated the condensation of HPO_4^{2-} to form $P_2O_7^{4-}$ species after H_3PO_4 treatment.[28]

FT-IR spectra of CaHAP and anion-modified CaHAP in the range of 1500−4000 cm^{-1} are shown in Figure 3c. The peaks at 1990, 2078, and 2148 cm^{-1} can be assigned to PO_4^{3-} combination and overtone bands.[33] The broad band in the region of 3500−3200 cm^{-1} is attributed to H bonding between OH^- and adsorbed water on the apatite.[34] The features at 3450 and 1630 cm^{-1} are due to adsorbed water. The intensity of the above bands is unchanged with WO_4^{2-} modification, while the intensity is slightly increased for SO_4^{2-}/CaHAP and considerably decreased for PO_4^{3-}/CaHAP. Interestingly, the peak at 3560 cm^{-1} almost disappeared for PO_4^{3-}/CaHAP, suggesting that the additional PO_4^{3-} species are anchored via OH^- groups of the CaHAP lattice. This result further confirms the structural modification of CaHAP with PO_4^{3-} to form $Ca_3(PO_4)_2$ as indicated by XRD analysis. Owing to the broad nature of the peak around this region, the presence of trace amount of CaHAP with apatite structure cannot be completely ruled out.

To further understand the surface species of CaHAP and anion modified CaHAP, Raman spectroscopy was employed (Figure 4). Raman spectroscopy can be used as a technique to distinguish between CaHAP and $Ca_3(PO_4)_2$ phases.[35] The main characteristic peaks of CaHAP were observed at 960, 1040, 1070, 580, and 426 cm^{-1}, with shoulders at 598 and 440 cm^{-1}. The major peak at 960 cm^{-1} is attributed to $\upsilon(PO_4^{3-})$ tetrahedron. Other peaks can be assigned to doubly degenerate, triply degenerate, and tetrahedron modes of PO_4^{3-} units. Several less intense peaks below 300 cm^{-1} are due to translational modes of CaHAP sublattices.

SO_4^{2-} modified CaHAP also exhibited similar features to CaHAP, while WO_4^{2-} modified CaHAP contains additional features at 908, 830, 790, 395, 329, 202, 110 cm^{-1}. It was

dx.doi.org/10.1021/jp304187v | J. Phys. Chem. C 2012, 116, 18736−18745

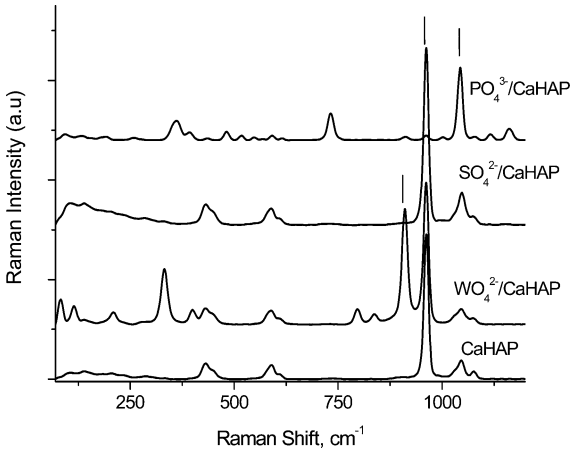

Figure 4. Raman spectral analysis of CaHAP and WO_4^{2-}, SO_4^{2-}, PO_4^{3-} modified CaHAP samples.

reported that crystalline features of WO_3 can be observed at 807 υ(O−W−O), 715 υ(O−W−O), 434 δ(O−W−O), 327 δ(O−W−O), 273 δ(O−W−O), 218 υ(W−O−W), and 134 (lattice mode) cm^{-1}.[36] However, none of these features closely match the additional bands observed in this study. In addition, there is no new peak at 970 cm^{-1} indicating the existence of isolated WO_3 species on the CaHAP surface. Therefore, the non-CaHAP features could be attributed to mineral scheelite (calcium tungstate $CaWO_4$).[37] It is important to note that no reflections in the XRD patterns indicating the formation of $CaWO_3$ phase have been observed. These results suggest the formation of small crystallites of scheelite in the sample. In the case of PO_4^{3-}/CaHAP sample, the intensity of the major peak observed for CaHAP at 960 cm^{-1} is significantly decreased and a new feature at 1040 cm^{-1} showed the highest intensity with additional features at 1080, 730, 478, 375, and 356 cm^{-1}. The peaks at 1005, 1045, and 1080 cm^{-1} can be attributed to the characteristic Raman features of β-TCP in the υ3 region.[35] In addition, two new features at 1160 and 1116 cm^{-1} can be observed in the spectrum. This is corroborated by the intensity decrease of the PO_4^{3-} ions at 962 cm^{-1} (symmetric stretch) and other peaks in the wavelength ranges of 400−450, 570−610, and 1020−1100 cm^{-1}. The unit cell of Ca_3PO_4 contains 42 PO_4^{3-} tetrahedra compared to 6 PO_4^{3-} tetrahedra for CaHAP. The Raman result of PO_4^{3-}/CaHAP is in good agreement with FT-IR results clearly suggesting the formation of new surface species with PO_4^{3-} interaction. It should be noted here that Raman spectra results showed the characteristic WO_4^{2-} peaks that could not be detected by FT-IR and XRD. The presence of WO_4^{2-} species in the Raman spectrum clearly indicates the substitution of WO_x^- in the CaHAP framework with a formula $Ca_{10}(PO_4)_{6-x}(WO_4)_x(OH)_2$.

DRIFTS Study of Ethanol Adsorption on Various CaHAP Samples. The DRIFT spectra collected after heat treatment of bulk CaHAP from room temperature (RT) to 400 °C are shown in Figure 5a,b. In the hydroxyl stretching region, peaks at 3670, 3570, and 3540 and a broad band with maximum around 3215 cm^{-1} were observed. Besides these typical CaHAP bands, two small peaks around 1420 and 1460 cm^{-1} were also observed due to the presence of carbonate $(CO_3)^{2-}$ impurities, that are not affected by the heat treatment up to 400 °C, suggesting that stable carbonates are formed in the CaHAP framework. The peak at 3670 cm^{-1} can be attributed to OH groups attached to phosphorus atoms in the apatite framework. On the other hand, the peak at 1630 cm^{-1} is attributed to molecularly adsorbed water. This peak as well as other peaks in the hydroxyl stretching region decrease in intensity with the increase in heating temperature.

The adsorption of ethanol on Ca-hydroxyapatite by in situ experiments was not thoroughly studied. Therefore, the DRIFT spectra were recorded under similar conditions to ethanol dehydration to further understand the mechanistic aspects of the reaction (Figure 6). Ethanol adsorbed on CaHAP for 15 min yielded peaks at 2975 νas(CH_3), 2930 νas(CH_2), and 2903 cm^{-1} νas (CH_3) corresponding to the ethoxy species. Further, a broad band was observed at 3250 cm^{-1} due to ν(OH) vibration of hydrogen bonded ethanol on CaHAP. The peak at 3665 cm^{-1} disappeared upon ethanol adsorption, indicating preferential ethanol adsorption on P−OH sites. The adsorption of ethanol at 400 °C resulted in much lower CH_x peaks intensity and showed partial recovery of the peak at 3665 cm^{-1},

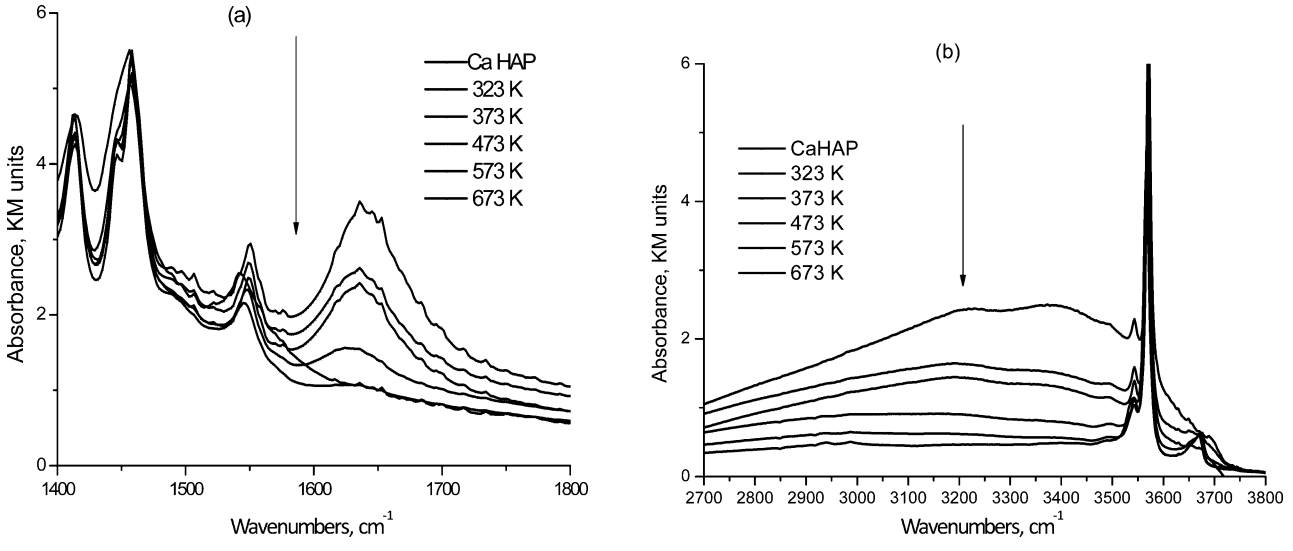

Figure 5. Thermal treatment of a CaHAP sample in the DRIFTS cell: (a) region between 2700 and 3800 cm^{-1}; (b) region between 1400 and 1800 cm^{-1}.

dx.doi.org/10.1021/jp304187v | J. Phys. Chem. C 2012, 116, 18736−18745

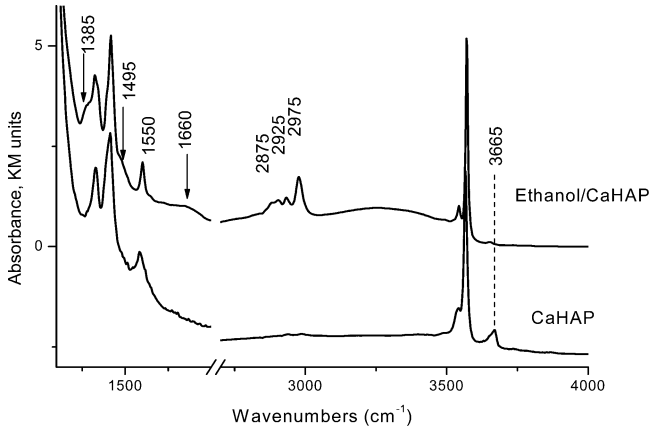

Figure 6. DRIFT spectra during ethanol adsorption on pure CaHAP.

suggesting the regeneration of the surface species. Upon ethanol adsorption, two new peaks at 1385 and 1495 cm^{-1} were observed indicating the formation of acetate species. These peaks can be attributed to CH_3CH_2O and CH_3COO^- adsorbed on the CaHAP surface, respectively.[38] The peak at 1660 cm^{-1}, which can be attributed to the υ(CO) mode of the acetate species, is also observed.[39] The presence of the acetyl species suggests the dehydrogenation capability of bulk CaHAP. The surface ethoxy species is converted to acetate by dehydrogenation to form acetaldehyde.[40] Upon heat treatment from ambient to 400 °C the intensity of the bands corresponding to ethoxy species decreased. This clearly demonstrates that the adsorbed ethanol decomposes to form products such as C_2H_4, CH_3CHO, CO, CH_4, H_2. Anions modified CaHAP samples also showed the characteristic ethoxy species at room temperature suggesting strong interaction of ethanol with the CaHAP surface (not shown here for the sake of brevity).

Surface Reactivity of Ethanol over Various CaHAP Catalysts. To understand the surface reactivity of modified CaHAP samples, ethanol-TPD was conducted from ambient temperature to 500 °C. Another objective of these experiments is to identify various products formed on anion modified CaHAP as compared to those formed on pristine CaHAP. Prior to ethanol adsorption, the sample was heated at 200 °C for 2 h in flowing He (30 mL/min). Ethanol was adsorbed in a continuous mode using a saturator with a constant He flow (50 mL/min). Ethanol-TPD results on various CaHAP catalysts are shown in Figure 7a–d. On pure CaHAP, the main products observed are acetaldehyde, ethylene, and diethyl ether (DEE). Acetaldehyde formation was observed at very low temperatures around 60 °C. Small amounts of ethylene and DEE were also observed at low temperatures. The high temperature desorption maximum of ethylene was observed at 265 °C. This result clearly indicates the ability of CaHAP to carry out both dehydrogenation and dehydration at low temperatures.

WO_4^{2-} modified CaHAP exhibited the highest acetaldehyde yield compared to the others indicating the preferential dehydrogenation pathway on this catalyst. Interestingly, a small amount of ethanol was also desorbed indicating less number of active sites available on this catalyst for the ethanol transformation. On the other hand, the PO_4^{3-}/CaHAP sample

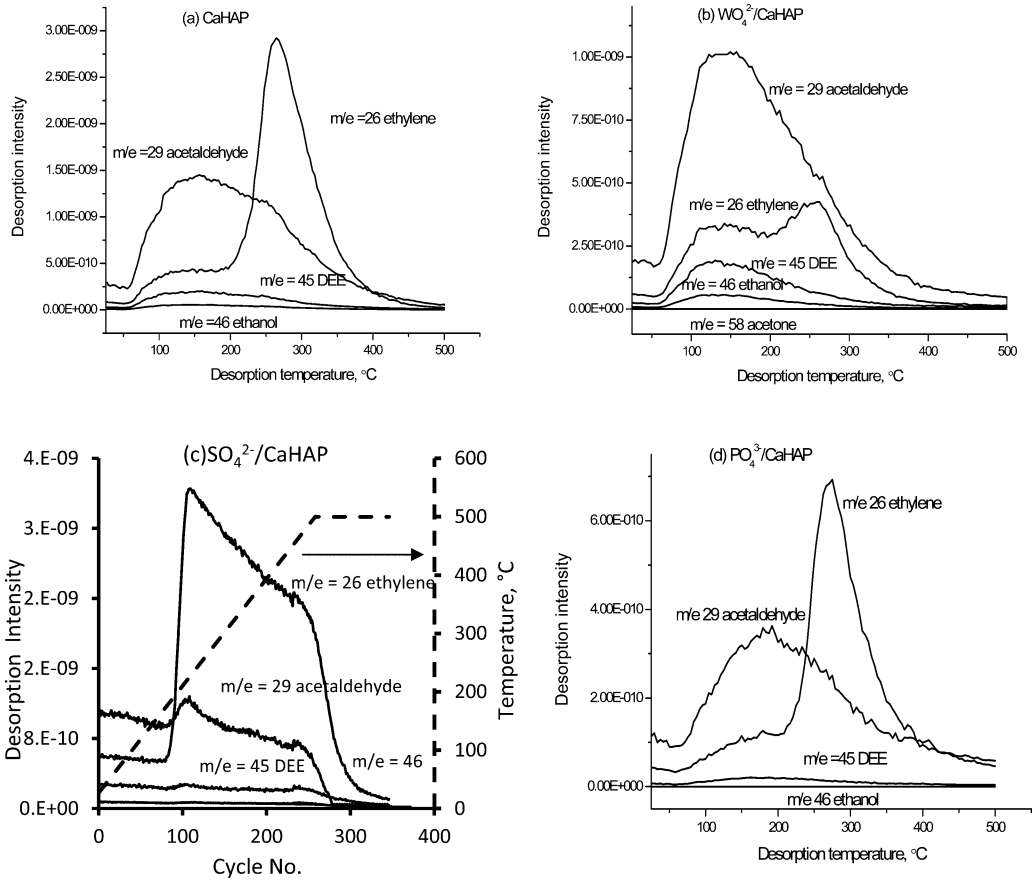

Figure 7. Product distribution in ethanol-TPD over (a) pure CaHAP, (b) WO_4^{2-}/CaHAP, (c) SO_4^{2-}/CaHAP, and (d) PO_4^{3-}/CaHAP.

dx.doi.org/10.1021/jp304187v | J. Phys. Chem. C 2012, 116, 18736–18745

yielded high ethylene in the product distribution. Ethylene desorption was often accompanied with two prominent desorption peaks around 150 and 300 °C. The low temperature peak at 150 °C often showed low intensity. Interestingly, diethyl ether (DEE) (*m*/*e* 45) also showed a small peak around 150 °C and displayed a similar peak shape to ethylene at 150 °C. The major ethylene desorption peak is centered at 300 °C, starting upon the completion of DEE desorption indicating the transformation of DEE to ethylene at relatively higher temperatures. It can be proposed that the low temperature peak due to ethylene at 150 °C is a result of direct intramolecular dehydration of ethanol forming ethylene. Thus, at low reaction temperatures, the formation of DEE indicates intramolecular dehydration of ethanol adsorbed on CaHAP catalysts. This result further suggests that at a low temperature below 250 °C, both intermolecular and intramolecular dehydrations take place simultaneously on PO_4^{3-}/CaHAP. In the case of PO_4^{3-}/CaHAP, no appreciable ethanol desorption is observed, indicating a strong interaction of ethanol on this sample. On the SO_4^{2-}/CaHAP sample, ethylene formation is higher compared to others, indicating preferential dehydration properties of this catalyst. The highest amount of H_2 was produced on WO_4^{2-}/CaHAP followed by CaHAP > PO_4^{3-}/CaHAP > SO_4^{2-}/CaHAP. The amounts of various gaseous products (CO, CH_4, CO_2, H_2) on different catalysts followed the trend CaHAP > PO_4^{3-}/CaHAP > SO_4^{2-}/CaHAP > WO_4^{2-}/CaHAP. No significant amount of acetone was detected on all tested samples.

Reactivity in Ethanol Conversion. To study the surface reactivity of CaHAP and WO_4^{2-}, SO_4^{2-}, and PO_4^{3-} modified CaHAP catalysts, a temperature-dependent ethanol conversion was conducted. Prior to the reaction, blank tests were conducted and no ethanol conversion was observed at the reaction temperature range investigated. CaHAP showed high initial activity that stabilizes only after 4 h. Therefore, we report the catalytic data for all materials after 4 h to be consistent. Figure 8 shows the reaction results of ethanol conversion over bulk CaHAP catalysts from 300 to 450 °C. Ethanol conversion increases with temperature, while selectivity toward diethyl ether decreases and ethylene is increased. This result clearly suggests that the CaHAP is capable of carrying out ethanol dehydration to form ethylene and DEE. On the other hand, acetaldehyde selectivity also increases with the reaction temperature, reaching 5.2% at 450 °C.

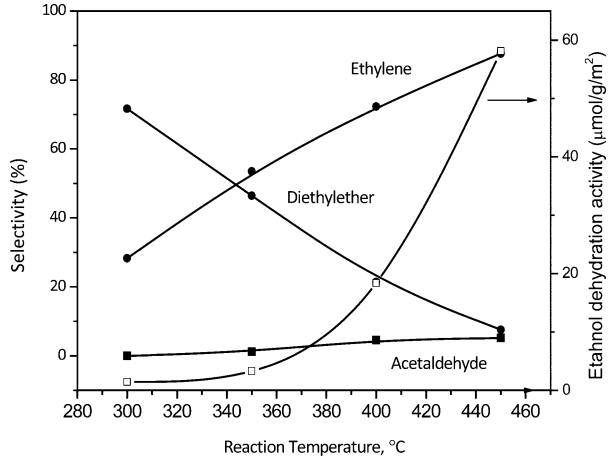

Figure 8. Ethanol conversion activity of CaHAP sample at various reaction temperatures.

To compare the catalytic activity of anion-modified CaHAP samples, the ethanol conversion was carried out at 400 °C and the following trend in catalytic activity was obtained: CaHAP > WO_4^{2-}/CaHAP > PO_4^{3-}/CaHAP > SO_4^{2-}/CaHAP. For comparison, the catalytic activity of various CaHAP catalysts is presented in Table 2. However, the dehydration selectivity to form ethylene and DEE showed the following trend: SO_4^{2-}/CaHAP ≥ CaHAP > PO_4^{3-}/CaHAP > WO_4^{2-}/CaHAP. Interestingly, ethylene formation was found to be the highest for SO_4^{2-}/CaHAP, followed by CaHAP, WO_4^{2-}/CaHAP, and PO_4^{3-}/CaHAP. Acetaldehyde formation by ethanol dehydrogenation was found to be the highest for WO_4^{2-}/CaHAP. The PO_4^{3-}/CaHAP sample showed the lowest dehydration and dehydrogenation activity, mainly producing higher olefins, dienes, aromatics, and parafins.

Table 2. Ethanol Dehydration Activity Results of CaHAP and WO_4^{2-}, SO_4^{2-}, and PO_4^{3-} Modified CaHAP Catalysts

		% selectivity		
sample	activity, μmol/h/m²	ethylene	DEE	acetaldehyde
CaHAP	18.4	73	22	5
WO_4^{2-}/CaHAP	7.2	71	2	10
SO_4^{2-}/CaHAP	5.5	85	10	2
PO_4^{3-}/CaHAP	6.6	27	7	5

Tanaka et al.[41] reported that the surface modification of hydroxyapatite with pyrophosphoric acid generated additional hydroxyl groups as follows: surface P−OH + $H_4P_2O_7$ → surface P−O−$PO(OH)_2$ + H_3PO_4. This newly formed phase for the samples with Ca/P ratios lower than 1.50 was transformed to β-$Ca_3(PO_4)_2$ when treated above 850 °C. However, in the present study, upon H_3PO_4 treatment, the CaHAP surface partially transformed to β-$Ca_3(PO_4)_2$ via $Ca_2P_2O_7$ formation.

The interaction of anions such as WO_4^{2-}, SO_4^{2-}, and PO_4^{3-} with CaHAP surface seems to modify the textural and structural properties of the CaHAP. The newly formed species influenced the CaHAP surface reactivity in the conversion of ethanol. Surface reactivity of alcohols on oxides is determined by various factors such as surface functional groups, acidic-basic properties, texture, and structural properties. As indicated by ethanol-TPD and ethanol conversion, the WO_4^{2-}/CaHAP catalysts exhibited high dehydrogenation activity in converting ethanol to acetaldehyde, whereas the SO_4^{2-}/CaHAP favored the dehydration route to form ethylene. CaHAP and PO_4^{3-}/CaHAP showed moderate dehydration and dehydrogenation activities. To our knowledge, this is the first report which describes the addition of WO_x on CaHAP surface and formation of $CaWO_4$ as evidenced by Raman spectra. The structure and surface properties of CaHAP samples were affected by anions addition.

5.0. CONCLUSIONS

In this work, we have synthesized the CaHAP by using $NH_4H_2PO_4$ and H_3PO_4 as phosphorus sources. The CaHAP synthesized from $NH_4H_2PO_4$ showed the presence of and carbonate species as evidenced in IR spectra. However, CaHAP prepared from H_3PO_4 only showed comparatively lesser amounts of carbonate species. Among various anion (WO_4^{2-}, SO_4^{2-}, and PO_4^{3-}) modified CaHAP samples, the crystallinity was only affected the addition of PO_4^{3-}. The addition of 10% PO_4^{3-} on CaHAP resulted in a significant modification of the

dx.doi.org/10.1021/jp304187v | J. Phys. Chem. C 2012, 116, 18736−18745

CaHAP surface, forming mainly $Ca_2P_2O_7$ and Ca_3PO_4 (β-TCP) as evidenced in XRD, FT-IR, and Raman. For the first time, we have observed the presence of WO_4^{2-} due to the formation of a mineral $CaWO_4$ phase, as indicated in the Raman spectrum for the WO_3 modified CaHAP sample. The anions-modified catalysts showed significantly different surface reactivity as compare to pure CaHAP. Pure CaHAP sample exhibited both dehydrogenation and dehydration properties. The formation of $Ca_3(PO_4)_2$ showed significantly lower ethanol conversion activity compare to CaHAP. WO_4^{2-}/CaHAP catalyst showed higher dehydrogenation activity compared to all other catalysts as evidenced by temperature programmed desorption of ethanol and ethanol conversion, while the SO_4^{2-}/CaHAP catalyst exhibited predominantly ethanol dehydration activity.

AUTHOR INFORMATION

Corresponding Author

*E-mail: kanaparthi_ramesh@hpcl.co.in.

Notes

The authors declare no competing financial interest.

ACKNOWLEDGMENTS

This work was supported by the Science and Engineering Research Council (SERC) of A*STAR (Agency for Science Technology and Research), Singapore.

REFERENCES

(1) Yamasaki, Y.; Yokoyama, A.; Ohnaka, A.; Kato, Y.; Murotsu, T.; Matsubara, K. *J. Chromatogr.* **1989**, *467*, 299−303.

(2) Zhou, W. Y.; Lee, S.; Wang, M.; Cheung, W. L.; Ip, W. Y. *J. Mater. Sci. Mater. Med.* **2008**, *19*, 2535−2540.

(3) Xu, J.; White, T.; Li, P.; He, C.; Han, Y. F. *J. Am. Chem. Soc.* **2010**, *132*, 1372.

(4) Han, Y. F.; Phonthammachai, N.; Ramesh, K.; Zhong, Z.; White, T. *Environ. Sci. Technol.* **2008**, *42* (3), 908−912.

(5) Matsumura, Y.; Moffat, J. B. *J. Catal.* **1994**, *148* (1), 323−33.

(6) Opre, Z.; Grunwaldt, J. D.; MacIejewski, M.; Ferri, D.; Mallat, T.; Baiker, A. *J. Catal.* **2005**, *230* (2), 406−419.

(7) Opre, Z.; Ferri, D.; Krumeich, F.; Mallat, T.; Baiker, A. *J. Catal.* **2007**, *251* (1), 48−58.

(8) Venugopal, A.; Scurrell, M. S. *Appl. Catal. A: Gen.* **2003**, *245* (1), 137−147.

(9) Jun, J. H.; Lee, T. J.; Lim, T. H.; Nam, S. W.; Hong, S. A.; Yoon, K. J. *J. Catal.* **2004**, *221* (1), 178−190.

(10) Elkabouss, K.; Kacimi, M.; Ziyad, M.; Ammar, S.; Bozon-Verduraz, F. *J. Catal.* **2004**, *226*, 16−24.

(11) Monma, H. *J. Catal.* **1982**, *75*, 200−203.

(12) Kibby, C. L.; Hall, W. K. *J. Catal.* **1973**, *29* (1), 144−159.13.

(13) Tsuchida, T.; Kubo, J.; Yoshioka, T.; Sakuma, S.; Takeguchi, T.; Ueda, W. *J. Catal.* **2008**, *259* (2), 183−189.

(14) Tsuchida, T.; Yoshioka, T.; Sakuma, S.; Takeguchi, T.; Ueda, W. *Ind. Eng. Chem. Res.* **2008**, *47* (5), 1443−1452.

(15) Hara, T.; Kanai, S.; Mori, K.; Mizukaki, T.; Ebitani, K.; Jitsukawa, K.; Kaneda, K. *J. Org. Chem.* **2006**, *71*, 7455−7462.

(16) Chickerur, N. S.; Mahapatra, P. P. *J. Inorg. Nucl. Chem* **1978**, *40*, 131.

(17) Boucetta, C.; Kacimi, M.; Ensuque, A.; Piquemal, J.-Y.; Bozon-Verduraz, F.; Ziyad, M. *Appl. Catal, A: Gen.* **2009**, *356* (2), 201−210.

(18) Ogo, S.; Onda, A.; Yanagisawa, K. *Appl. Catal. A: Gen.* **2008**, *348* (1), 129−134.

(19) Onda, A.; Ogo, S.; Kajiyoshi, K.; Yanagisawa, K. *Mater. Lett.* **2008**, *62* (8−9), 1406−1409.

(20) Tanaka, H.; Futaoka, M.; Hino, R.; Kandori, K.; Ishikawa., T. *J. Colloid Interface Sci.* **2005**, *283*, 609−612.

(21) Matsumura, Y.; Moffat, J. B. *J. Chem. Soc. Faraday Trans.* **1996**, *92* (11), 1981−1984.

(22) Choi, H. W.; Lee, H. J.; Kim, K. J.; Kim, H. M.; Lee, S. C. *J. Colloid and Interface Sci.* **2006**, *304*, 277−281.

(23) Liao, C. J.; Lin, F. H.; Chen, K. S.; Sun, J. S. *Biomaterials.* **1999**, *20*, 1807−1813.

(24) Kim, W.; Saito, F. *Ultrason. Sonochem.* **2001**, *8*, 85−88.

(25) Kumta, P. N.; Sfeir, C.; Lee, D. H.; Olton, D.; Choi, D. *Acta Biomater.* **2005**, *1*, 65−83.

(26) Ashok, J.; Naveen Kumar, S.; Subrahmanyam, M.; Venugopal, A. *Catal. Lett.* **2008**, *121*, 283.

(27) Cantero, M.; Moreno Real, L.; Bruque, S.; Martinez Lara, M.; Ramos Barrado, J. R. *Solid State Ionics* **1992**, 273.

(28) Cacciotti., I.; Bianco, A. *Ceram. Int.* **2011**, 37−127−137.

(29) Dominez, M. I.; Romero-Sarria, F.; Centeno, M. A.; Odriozola, J. A. *Appl. Catal. B Environ.* **2009**, *87*, 245−251.

(30) Wei, C.; Zhiliang, H.; Yu, L.; Qianjun, H. *Catal. Commun.* **2008**, *9*, 516−521.

(31) Boukha, Z.; Kacimi, M.; Periera, M. F. R.; Faria, J. L.; Figueiredo, J. L.; Ziyad, M. *Appl. Catal. A: Chem.* **2007**, *317*, 299.

(32) Raynaud, S.; Champion, D.; Bernache-Assollant, B.; Thomas, P. *Biomaterials* **2002**, *23*, 1065−1072.

(33) Joris, S. J.; Amberg, C. H. *J. Phys. Chem.* **1971**, *75*, 3167−3172.

(34) Solhy, A.; Tahir, R.; Sebti, S.; Skouta, R.; Bousmina, M.; Zahouily, M.; Larzek, M. *Appl. Catal.* **2010**, *374*, 189−193.

(35) de Aza, P. N.; Guitian, F.; Santos, C.; de Aza, S.; Cusco, R.; Artus, L. *Chem. Mater.* **1997**, *9*, 916−922.

(36) Daniel, M. F.; Desbat, B.; Lassegues, J. C.; Gerand, B.; Figlarz, M. *J. Solid State Chem.* **1987**, *67*, 235.

(37) Frost, R. L.; Duong, L.; Weier, M. *Spectrochim. Acta A* **2004**, *60*, 1853.

(38) Yu., Z.; Chuang, S. C. *J. Catal.* **2007**, *246*, 118−126.

(39) Mattos, L. V.; Noronha, F. B. *J. Catal.* **2005**, *203*, 453.

(40) de Lima, S. M.; da Silva, A. M.; da Costa, L. O. O.; Graham, U. M.; Jacobs., G.; Davis, B. H.; Mattos, L. V.; Norornha, F. B. *J. Catal.* **2009**, *268*, 268−281.

(41) Tanaka, H.; Futaoka, M.; Hino, R. *J. Colloid Interface Sci.* **2004**, *269*, 358−363.